

©2019 IEEE. Personal use of this material is permitted. Permission from IEEE must be obtained for all other uses, in any current or future media, including reprinting/republishing this material for advertising or promotional purposes, creating new collective works, for resale or redistribution to servers or lists, or reuse of any copyrighted component of this work in other works.

Digital Object Identifier [10.1109/TPEL.2019.2896707](https://doi.org/10.1109/TPEL.2019.2896707)

IEEE Transactions on Power Electronics

Robust stability analysis of synchronverters operating in parallel

Roberto Rosso

Soenke Engelken

Marco Liserre

Suggested Citation

R. Rosso, S. Engelken and M. Liserre, "Robust Stability Analysis of Synchronverters Operating in Parallel," in IEEE Transactions on Power Electronics, vol. 34, no. 11, pp. 11309-11319, Nov. 2019.

Robust Stability Analysis of Synchronverters Operating in Parallel

Roberto Rosso, *Student Member, IEEE*, Soenke Engelken, *Member, IEEE*, and Marco Liserre, *Fellow, IEEE*

Abstract—Recent studies have shown how synchronization units of converters operating nearby may interact with each other, affecting the stability of the system. Synchronverters are able to self-synchronize to the grid without the need of a dedicated unit because they can reproduce the power synchronization mechanism of synchronous machines (SMs). Recently, the robust stability of a synchronverter has been investigated by means of structured singular values (SSV or μ -analysis). In this paper, μ -analysis is performed to investigate how the robust stability of a synchronverter is affected by the presence of another converter of the same type operating in parallel. It is demonstrated that the parallel operation of synchronverters reduces their robust stability and a possible solution is proposed, based on the implementation of virtual impedances in the control algorithm. An accurate state-space model of the system under study is developed by adopting the component connection method (CCM) and the robust stability analysis is validated against time-domain simulations in MATLAB/Simulink/PLECS and experimental results with a power-hardware in the loop (PHIL) test bench.

Index Terms—Parallel operation of synchronverters, synchronverter robust stability analysis, μ -analysis, virtual impedance, structured singular values.

I. INTRODUCTION

The growth of power electronics-based generation has raised concerns among system operators about power system stability. New control strategies, which guarantee stable operation of the system even in scenarios with high penetration of inverters are requested. Virtual synchronous machines (VSMs) have been proposed as possible solutions and their capability to self-synchronize themselves to the main utility grid without the need of a dedicated unit is appealing [1]-[6]. In fact, recent studies have shown that the synchronization unit of a grid connected converter has a significant impact on the frequency behaviour of the converter itself, with consequences for its stability [7], [8]. Furthermore, interaction between synchronization units of converters operating nearby may occur, especially under weak grid conditions [9]. The synchronverter presented in [2] is among the most popular VSM implementations. Its stability and dynamic performance have been investigated in the literature [10]-[13] and modifications to the original control structure have been proposed [6], [14].

In recent years, the impedance-based stability criterion has been extensively adopted for stability analysis of grid connected converters [15], [16]. This approach has been used in [17] for stability analysis of a synchronverter-based wind farm. However, synchronverter stability and design have been mainly studied by means of eigenvalues analysis in the literature, where linearized models of the system have

been adopted for the investigation [10]-[13]. Nevertheless, due to the multi-input multi-output (MIMO) nature of the studied system, multivariable analysis is required in order to provide an estimation of the stability margin of the system [18], [19]. In fact, it is well known that eigenvalues are a poor measure of gain for MIMO systems, since they provide only information about a specific system configuration and do not take into account interactions between inputs and outputs of different channels [18]. Recently, the robust stability of a synchronverter was investigated by means of structured-singular values (SSVs) (commonly called μ -analysis) [20]. This approach is particularly suitable for introducing plant uncertainties in the analysis. In fact, due to the significant variations of characteristics and number of generation units and loads during the day, the common representation of the grid by means of a Thévenin equivalent at the connection point with a resistive-inductive impedance is often not sufficiently accurate [21].

Due to the intrinsic droop characteristic of synchronverters regulating power sharing among operating units, it is often taken for granted that synchronverters should not encounter particular problems when operating in parallel. However, this aspect has not yet been properly investigated in the literature. In [22], a non-linear model of a synchronverter-dominated microgrid is presented and the stability of the system is studied by means of bifurcation theory. [23] analyzes the behaviour of synchronverters operating in parallel by means of eigenvalue analysis and a linearized state-space model of multiple synchronverters operating in parallel is developed by means of the so-called component connection method (CCM) [24], so as linear control theory can be adopted for system stability assessment. The CCM technique allows connecting state-space representations of separated subsystems in a modular manner, such that the analysis can be easily extended to multiple operating units. The objective of this work is the investigation of the robust stability of synchronverters operating in parallel by means of μ -analysis. Similarly to [10], the system is split into two parts, namely the control and the plant, whose model is obtained adopting the approach presented in [23]. The presence of one or more units connected in parallel affects the characteristics of the plant where the synchronverter is connected, with consequent effects on system stability.

This paper is structured as follows: the system under study is introduced in Section II, along with the CCM technique adopted to obtain the state-space representation of the system. In Section III, the concept of μ -analysis is briefly introduced and then applied to the investigated case. In Section IV, experimental results performed with a power-hardware in the

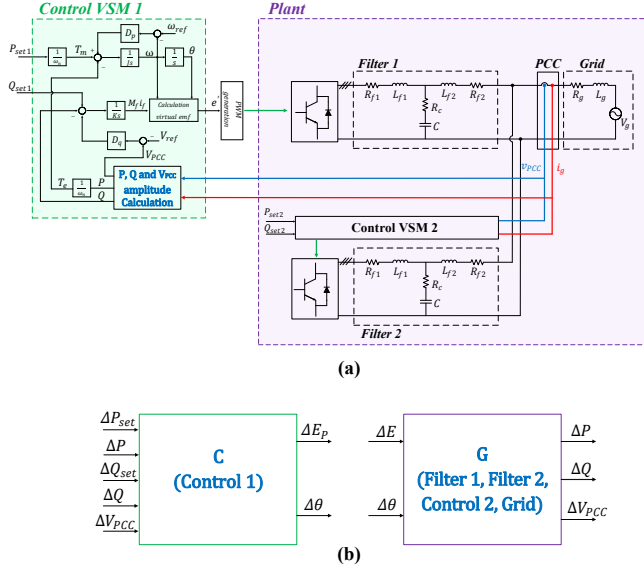


Figure 1. (a) Scheme of the studied system, (b) inputs and outputs of the linearized control and plant model.

loop (PHIL) test bench are reported and the developed model is validated against time-domain simulations and measurement. Section V is dedicated to the conclusions.

II. MODELLING OF THE SYSTEM

A scheme of the system under study is shown in Fig. 1 (a). It is composed of two inverters with their respective controls and output filters, sharing the same point of common coupling (PCC). Similarly to [20], in order to perform the μ -analysis, the system is split into two parts, namely the control and the plant, whose inputs and outputs are shown in Fig. 1 (b). Differently from [20], the plant not only consists of the converter filter and the grid, but it also includes the control and the filter of the second synchronverter connected in parallel. Nevertheless, the small-signal model presented in [20] cannot be extended easily to the case of multiple synchronverters operating in parallel, since the state-space representation of the control and the plant, obtained through linearization of the respective equations, has been adapted to the specific case. The most efficient way for including other inverters in the analysis is to adopt the CCM technique [23], [24]. It consists of connecting state-space representations of several subsystems in a modular manner, such that the analysis can be extended easily to a more complex system. The state-space representation of the overall system is therefore obtained by connecting to each other independent subsystems by means of the so-called interconnection matrices. The approach presented in this paper is based on [23], where the CCM was used to obtain the linearised model of two synchronverters operating in parallel. However, differently from [23], here the CCM is used in order to obtain the model of the plant G indicated in Fig. 1 (b).

In Fig. 2, the block diagram representation of the overall system under study is shown, along with inputs and outputs of each subsystem. The dark red and dark blue arrows indicate inputs and outputs of the plant, labelled as u_{plant} and y_{plant} ,

respectively. The state-space representation of the plant is given below:

$$\begin{cases} \dot{x}_{plant} = F_{int} x_{plant} + G_{int} u_{plant} \\ y_{plant} = H_{int} x_{plant} + J_{int} u_{plant} \end{cases}, \quad (1)$$

where F_{int} , G_{int} , H_{int} and J_{int} are defined as:

$$\begin{cases} F_{int} = A_d + B_d L_{11} (I - D_d L_{11})^{-1} C_d \\ G_{int} = B_d L_{11} (I - D_d L_{11})^{-1} D_d L_{12} + B_d L_{12} \\ H_{int} = B_d L_{21} (I - D_d L_{11})^{-1} C_d \\ J_{int} = L_{21} (I - D_d L_{11})^{-1} D_d L_{12} + L_{22} \end{cases}. \quad (2)$$

A_d , B_d , C_d and D_d are sparse block diagonal matrices obtained from the state-space matrices of the single subsystems, namely:

$$\begin{cases} A_d = \text{diag}\{A_{c2}, A_{LCL1}, A_{LCL2}, A_g, A_{PQ}\} \\ B_d = \text{diag}\{B_{c2}, B_{LCL1}, B_{LCL2}, B_g, B_{PQ}\} \\ C_d = \text{diag}\{C_{c2}, C_{LCL1}, C_{LCL2}, C_g, C_{PQ}\} \\ D_d = \text{diag}\{D_{c2}, D_{LCL1}, D_{LCL2}, D_g, D_{PQ}\} \end{cases}, \quad (3)$$

whereas L_{11} , L_{12} , L_{21} and L_{22} represent the aforementioned interconnection matrices, indicating how inputs and outputs of the sub-systems are connected to each other. Defining $u_{sub} = [u_{c2} \ u_{LCL1} \ u_{LCL2} \ u_g \ u_{PQ}]^T$ as the vector containing all the inputs of the subsystems and $y_{sub} = [y_{c2} \ y_{LCL1} \ y_{LCL2} \ y_g \ y_{PQ}]^T$ as the vector containing all the outputs, the following relation is valid:

$$\begin{cases} u_{sub} = L_{11} y_{sub} + L_{12} u_{plant} \\ y_{plant} = L_{21} y_{sub} + L_{22} u_{plant} \end{cases}, \quad (4)$$

where u_{plant} and y_{plant} are the vectors containing inputs and outputs of the interconnected system, namely $u_{plant} = [\Delta E \ \Delta \theta]^T$ and $y_{plant} = [\Delta P_1 \ \Delta Q_1 \ \Delta V_{PCC}]^T$. According to [23], the state-space representation of each subsystem of Fig. 2 is provided in the following.

A. Control

The description of the synchronverter control, along with its state-space representation are reported in [10]. The state-space matrices A_c , B_c , C_c and D_c of the control block in Fig. 2 are shown below:

$$\begin{aligned} A_c &= \begin{bmatrix} 0 & 0 & 0 \\ 0 & -\frac{D_p}{J} & 0 \\ 0 & 1 & 0 \end{bmatrix}; \quad B_c = \begin{bmatrix} 0 & 0 & \frac{1}{K} & -\frac{1}{K} & -\frac{D_q}{K} \\ \frac{1}{\omega_0 J} & -\frac{1}{\omega_0 J} & 0 & 0 & 0 \\ 0 & 0 & 0 & 0 & 0 \end{bmatrix}; \\ C_c &= \begin{bmatrix} \omega_0 & M_f i_{f0} & 0 \\ 0 & 0 & 1 \end{bmatrix}; \quad D_c = [0^{2 \times 5}]. \end{aligned} \quad (5)$$

D_p , D_q , K and J are the control parameters shown in the control block diagram in Fig 1 (a), whereas ω_0 and $M_f i_{f0}$ are initial conditions of the system states [10].

B. LCL Filter

Choosing the current of the converter side inductor i_{L1} , the current of the grid side inductor i_{L2} and the capacitor voltage

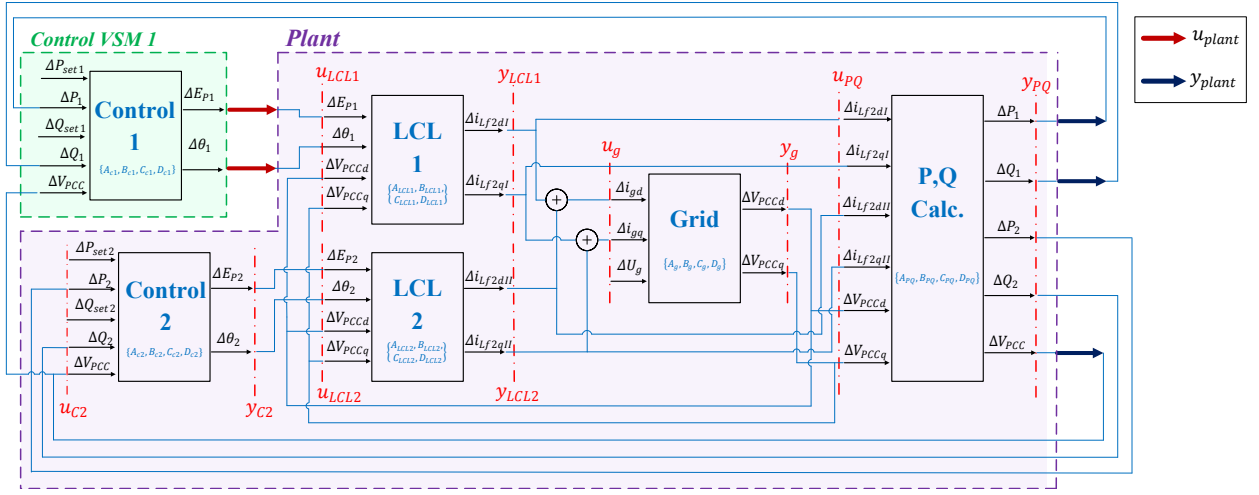


Figure 2. Structure of the system for CCM analysis.

v_c as state space variables of the subsystem, the equations of the LCL filter shown in Fig. 1 are reported below [10]:

$$\begin{cases} L_{f1} \frac{di_{L1}}{dt} = e - v_c - R_c(i_{L1} - i_{L2}) - R_{f1}i_{L1} \\ C \frac{dv_c}{dt} = i_{L1} - i_{L2} \\ L_{f2} \frac{di_{L2}}{dt} = v_c - v_{PCC} + R_c(i_{L1} - i_{L2}) - R_{f2}i_{L2} \end{cases} \quad (6)$$

Writing (6) in dq coordinates, the following state-space matrices A_{LCL} , B_{LCL} , C_{LCL} and D_{LCL} are obtained:

$$A_{LCL} = \begin{bmatrix} \frac{-R_c - R_{f1}}{L_{f1}} & \omega_0 & -\frac{1}{L_{f1}} & 0 & \frac{R_c}{L_{f1}} & 0 \\ -\omega_0 & \frac{-R_c - R_{f1}}{L_{f1}} & 0 & -\frac{1}{L_{f1}} & 0 & \frac{R_c}{L_{f1}} \\ \frac{1}{C_f} & 0 & 0 & \omega_0 & -\frac{1}{C_f} & 0 \\ 0 & \frac{1}{C_f} & -\omega_0 & 0 & 0 & -\frac{1}{C_f} \\ \frac{R_c}{L_{f2}} & 0 & \frac{1}{L_{f2}} & 0 & \frac{-R_c - R_{f2}}{L_{f2}} & \omega_0 \\ 0 & \frac{R_c}{L_{f2}} & 0 & \frac{1}{L_{f2}} & -\omega_0 & \frac{-R_c - R_{f2}}{L_{f2}} \end{bmatrix}$$

$$B_{LCL} = \begin{bmatrix} \frac{\cos \theta_0}{L_{f1}} & -\frac{V_0 \sin \theta_0}{L_{f1}} & 0 & 0 \\ \frac{\sin \theta_0}{L_{f1}} & -\frac{V_0 \cos \theta_0}{L_{f1}} & 0 & 0 \\ 0 & 0 & 0 & 0 \\ 0 & 0 & 0 & 0 \\ 0 & 0 & -\frac{1}{L_{f2}} & 0 \\ 0 & 0 & 0 & -\frac{1}{L_{f2}} \end{bmatrix};$$

$$C_{LCL} = \begin{bmatrix} 0 & 0 & 0 & 0 & 1 & 0 \\ 0 & 0 & 0 & 0 & 0 & 1 \end{bmatrix}; \quad D_{LCL} = [0^{2 \times 4}]. \quad (7)$$

C. Grid

The grid has been modelled using its Thévenin equivalent at the PCC. In order to obtain the information about the voltage at the connection point, another state has been introduced in the grid model, namely a shunt capacitor at the input terminal as shown in Fig. 3. Choosing very high values for the shunt components R_s and C_s , so that all the current i_g flows into

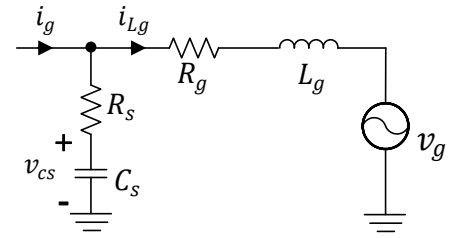


Figure 3. Equivalent grid model.

the grid, the PCC voltage is represented by the voltage v_{cs} across the shunt capacitor. The corresponding grid equations are provided below:

$$\begin{cases} L_g \frac{di_{Lg}}{dt} = R_s(i_g - i_{Lg}) + v_{cs} - v_g - R_g i_{Lg} \\ C_s \frac{dv_{cs}}{dt} = i_g - i_{Lg} \end{cases}, \quad (8)$$

which transformed in dq coordinates result in the following state-space matrices of the grid subsystem:

$$A_g = \begin{bmatrix} \frac{-R_s - R_g}{L_g} & \omega_0 & \frac{1}{L_g} & 0 \\ -\omega_0 & \frac{-R_s - R_g}{L_g} & 0 & \frac{1}{L_g} \\ -\frac{1}{C_s} & 0 & 0 & \omega_0 \\ 0 & -\frac{1}{C_s} & -\omega_0 & 0 \end{bmatrix}; \quad B_g = \begin{bmatrix} \frac{R_s}{L_g} & 0 & -1 \\ 0 & \frac{R_s}{L_g} & 0 \\ \frac{1}{C_s} & 0 & 0 \\ 0 & \frac{1}{C_s} & 0 \end{bmatrix};$$

$$C_g = \begin{bmatrix} 0 & 0 & 1 & 0 \\ 0 & 0 & 0 & 1 \end{bmatrix}; \quad D_g = [0^{2 \times 3}]. \quad (9)$$

D. P, Q and V_{PCC} calculation

Calculation of active and reactive power of each converter, along with the amplitude of the PCC voltage involve algebraic equations. In order to obtain a state-space formulation out of these calculations, a first-order low pass filter with a very high cut-off frequency ω_c is introduced in the calculation of ΔP , ΔQ and ΔV_{PCC} reported in [10]:

$$\begin{cases} \Delta P = \left(\frac{\omega_c}{s+\omega_c}\right)^3 \frac{1}{2} (I_{Lf2d0} \Delta v_{PCCd} + I_{Lf2q0} V_{PCCq} + \\ \quad + V_{PCCd0} \Delta i_{Lf2d} + V_{PCCq0} \Delta i_{Lf2q}) \\ \Delta Q = \left(\frac{\omega_c}{s+\omega_c}\right)^3 \frac{1}{2} (-I_{Lf2d0} \Delta v_{PCCd} + I_{Lf2d0} V_{PCCq} + \\ \quad + V_{PCCq0} \Delta i_{Lf2d} - V_{PCCd0} \Delta i_{Lf2q}) \\ \Delta V_{PCC} = \left(\frac{\omega_c}{s+\omega_c}\right) \frac{V_{PCCd0} \Delta v_{PCCd} + V_{PCCq0} \Delta v_{PCCq}}{\sqrt{V_{PCCd0}^2 + V_{PCCq0}^2}} \end{cases}, \quad (10)$$

where the quantities with the subscript "0" indicate the values at the operating point and $i_{Lf2dq} = \{i_{Lf2dq1}, i_{Lf2dq2}\}$. The corresponding state-space matrices are provided below:

$$\begin{aligned} A_{PQ} &= \omega_c [I^{(5)}]; \quad C_{PQ} = [I^{(5)}]; \quad D_{PQ} = [0^{5 \times 6}] \\ B_{PQ} &= \omega_c \frac{3}{2} \begin{bmatrix} I_{Lf2dI0} & I_{Lf2qI0} & V_{d0} & V_{q0} & 0 & 0 \\ -I_{Lf2qI0} & I_{Lf2dI0} & V_{q0} & -V_{d0} & 0 & 0 \\ I_{Lf2dII0} & I_{Lf2qII0} & 0 & 0 & V_{d0} & V_{q0} \\ -I_{Lf2qII0} & I_{Lf2dII0} & 0 & 0 & V_{q0} & -V_{d0} \\ \frac{V_{d0}}{\Delta} & \frac{V_{q0}}{\Delta} & 0 & 0 & 0 & 0 \end{bmatrix}; \end{aligned} \quad (11)$$

where $V_{dq0} = V_{PCCdq0}$ and $\Delta = \sqrt{V_{PCCd0}^2 + V_{PCCq0}^2}$.

E. Interconnection matrices

L_{11} , L_{12} , L_{21} and L_{22} in (4) are sparse matrices of zeros and ones accounting for the connection among inputs and outputs of the subsystems composing the overall interconnected system. These are reported in the Appendix of the paper and below only their sizes are shown:

$$\begin{cases} u_{sub} = [L_{11}]^{22 \times 13} y_{sub} + [L_{12}]^{22 \times 2} u_{plant} \\ y_{plant} = [L_{21}]^{3 \times 13} y_{sub} + [L_{22}]^{3 \times 2} u_{plant} \end{cases}. \quad (12)$$

Although already defined at the beginning of this section, u_{sub} , u_{plant} , y_{sub} and y_{plant} are reported below for simplicity, where the notations of Fig. 2 for inputs and outputs of each subsystem are adopted:

$$\begin{cases} u_{sub} = [u_{c2} \ u_{LCL1} \ u_{LCL2} \ u_g \ u_{PQ}]^T \\ y_{sub} = [y_{c2} \ y_{LCL1} \ y_{LCL2} \ y_g \ y_{PQ}]^T \\ u_{plant} = [\Delta E_{p1} \ \Delta \theta_1]^T \\ y_{plant} = [\Delta P_1 \ \Delta Q_1 \ \Delta V_{PCC}]^T \end{cases}. \quad (13)$$

III. ROBUST STABILITY ANALYSIS

A. Introduction to μ -analysis

Eigenvalue analysis is among the commonly adopted approaches for stability assessment of grid connected converters and generally for power systems studies [25]. By means of modal analysis, the states mainly contributing to the oscillatory modes of a large interconnected system can be determined

[25], [27]. For instance, this approach has been adopted in [23] in order to investigate parallel operation of synchronverters. Although through eigenvalue analysis system stability can be efficiently assessed, it is well known that for MIMO systems, eigenvalues are a poor measure of robustness [18]. Indeed, eigenvalues provide only information about a specific configuration of the system when inputs and outputs are in the same direction, namely the direction of the eigenvectors. They do not take into account the possible interactions between different channels that typically occur in a MIMO system. For SISO analysis, gain and phase margin are identified as indicators of robustness. However, the definition of phase and gain margin of SISO systems cannot be easily extended to MIMO systems. For this reason, for accurate robustness assessment of MIMO systems, multivariable analysis is required and different methods have been developed, such as the structured singular values (SSV) or μ -analysis [18]-[20]. To this extent, singular values provide better information about the gains of the plants and the robustness of the control is verified against a defined set of system uncertainties. This method allows to span a set of possible system configurations instead of verifying stability only for a specific condition.

In [20], the robust stability of a synchronverter connected to the grid through an LCL filter has been investigated by means of μ -analysis. The calculated μ -factor provides an indication of system stability, namely the inverse of the highest peak of μ over the investigated frequency range represents the stability margin of the system [18]-[20]. The results of the performed analysis are strongly related to the chosen plant uncertainty and, in [20], a multiplicative input uncertainty with specific characteristics has been defined. Among the results presented in [20], the fact that the robust stability of the synchronverter is augmented when the converter is connected to a weaker grid is probably the most interesting one. In fact, this represents an opposite trend compared to the behaviour shown by converters relying on dedicated synchronization units [9]. In the following, the μ -analysis performed in [20] is extended to the case of two synchronverters operating in parallel. The presence of the second synchronverter modifies the characteristics of the plant with consequences on the results obtained in [20].

Table I
SIMULATION PARAMETERS

Description	Symbol	Value
Inverter rated power	$S_{n1}=S_{n2}$	300 kVA
Line-to-line voltage	V_{LL}	400 V (rms)
Rated grid frequency	f_g	50 Hz
Grid inductance	L_g	0.05 pu
Inverter-side filter inductance	$L_{f1I}=L_{f1II}$	0.08 pu
Grid-side filter inductance	$L_{f2I}=L_{f2II}$	0.02 pu
Grid resistance	R_g	0.005 pu
Inverter-side filter resistance	$R_{f1I}=R_{f1II}$	0.02 pu
Grid-side filter resistance	$R_{f2I}=R_{f2II}$	0.02 pu
Capacitor damping resistance	$R_{cI}=R_{cII}$	0.18 pu
Filter capacitor	$C_I=C_{II}$	0.05 pu
Virtual inertia	$J_1=J_2$	0.6687
K factor	$K_1=K_2$	37459
P-Droop coefficient	$D_{p1}=D_{p2}$	60.8 (5%)
Q-Droop coefficient	$D_{q1}=D_{q2}$	18371 (5%)

B. Application to the system under study

The same operating conditions of the converter considered in [20] are assumed for the analysis. Filter and control parameters of the two synchronverters are reported in Table I, whereas the considered frequency dependent uncertainty function is shown in Fig. 4. It presents an amplitude of 50% at low frequency, increasing till 500% at very high frequencies. This accounts for low frequency uncertainties due to parametric uncertainty in the model as well as high frequency neglected dynamic effects or resonances in the grid due to the presence of other converters operating nearby.

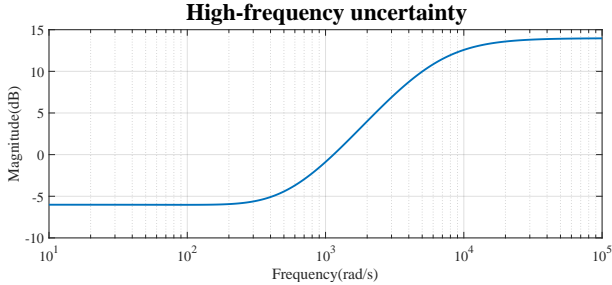


Figure 4. Multiplicative input uncertainty used for the μ -analysis.

In Fig. 5, the μ -factor over the investigated frequency range related to the defined set of plant uncertainties is shown. The blue curve indicates the results when the converter operates alone, while the red curve correspond to the parallel operation. The results clearly show how the highest peak of μ of approximately 0.61 at a frequency of 277 rad/s is shifted to a value of $\mu \approx 0.65$ at the same frequency for parallel operation, corresponding to a reduction of the stability margin.

In Fig. 6 (a) and (b), the μ -factor for a sweep of the grid SCR from 20 to 2 is shown for both examined cases. When the synchronverter operates alone, the increase of the

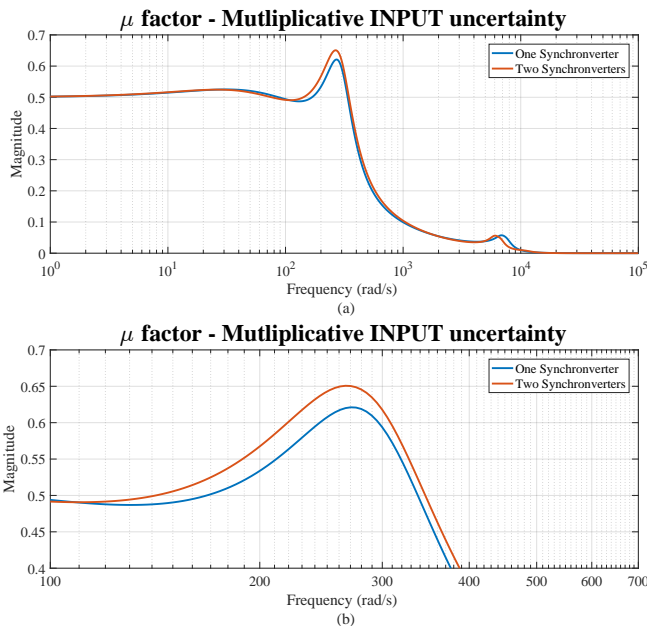


Figure 5. μ factor; (a) whole frequency range, (b) zoom.

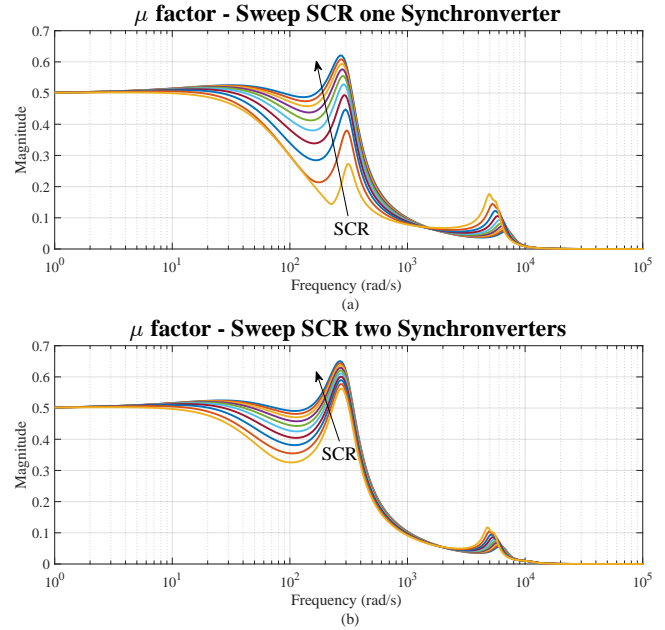


Figure 6. μ factor, sweep SCR from 20 to 2; (a) one synchronverter, (b) two synchronverters.

impedance between the converter and the grid enhances the robust stability of the converter against high frequency uncertainties in the plant. This has been justified in [20] by the fact that a synchronverter reproduces the behaviour of a real SM and basically behaves as a voltage source behind an impedance. The increase of the impedance between the voltage source and the grid produces the effects of a stability margin improvement [6]. Fig. 6 (b) clearly shows how the increase of the grid impedance does not produce the same effects when the synchronverter is operating in parallel with a second synchronverter. In fact, the other synchronverter nearby also behaves as a grid forming unit [28], reducing the benefits provided by the higher impedance between the converter and the grid.

C. Possible countermeasure

The analysis performed in the previous section has highlighted that the stability margin of a synchronverter is reduced when operating in parallel to a converter of the same type. The issue related to parallel operation is not only confined to synchronverters, but this is a general challenge for power electronics-based converters. Interactions among current controls and filters have been extensively investigated in the literature [15], [26], [27], along with the negative effects of synchronization units on the converter stability which has been addressed in several works [7], [8], [16]. Since synchronverters do not require a dedicated unit for their synchronization to the grid, the issues related to interactions among synchronization units of converters operating in parallel observed in [9] and [29] can be avoided. Although the control loops of a synchronverter are different from those of standard grid connected converters using dedicated synchronization units, the results of the analysis performed in this work show that the parallel operation among these types of converters has also effects on

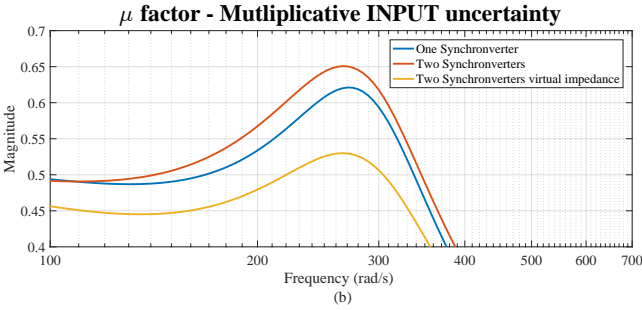
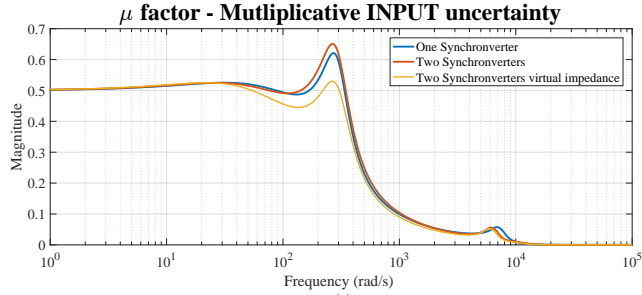


Figure 7. μ factor; (a) whole frequency range, (b) zoom.

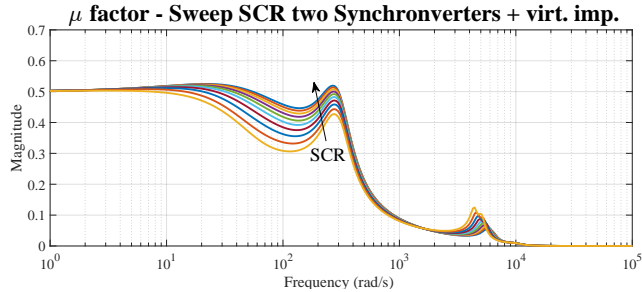


Figure 8. μ factor, sweep SCR from 20 to 2; (a) two synchronverters, (b) two synchronverters and increased filter impedance of 20%.

their stability. According to the considerations reported in the previous subsections and in [20], the impedance between the synchronverter and any other equivalent voltage source operating nearby has to be increased in order to enhance its robust stability. This can be interpreted as the need for an increase of the electrical distance between the two voltage sources. It is however important to point out that the synchronverter is not the only control structure proposed in the literature based on the power synchronization mechanism of a SM. In [30], a generalized formulation for power synchronization-based control algorithms has been presented and the results shown in this paper can be extended to such generalized structure.

Typical values of stator impedance of real SMs are generally much higher than the output impedance of standard converter filters. Normally, synchronous reactances of SMs are in the range of 1.5 to 2 pu [25], whereas the output impedance of a converter filter is generally significantly lower (in the range of 0.1-0.2 pu) [6]. Hence, the effects of an increase of filter parameters on the the μ -factor are reported in Fig. 7. The blue and red curves already shown in Fig. 5 are compared to the yellow curve accounting for the results of the μ -analysis obtained when the converter filter impedances of both synchronverters have been increased by 20%. The results

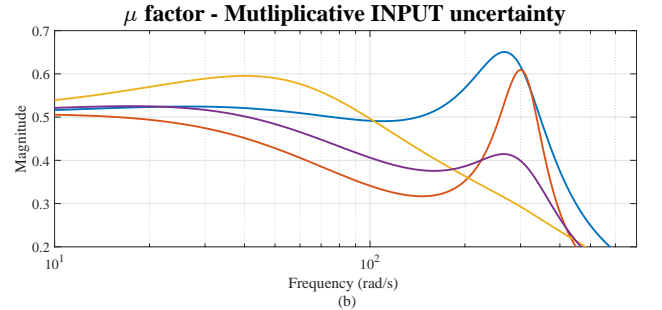
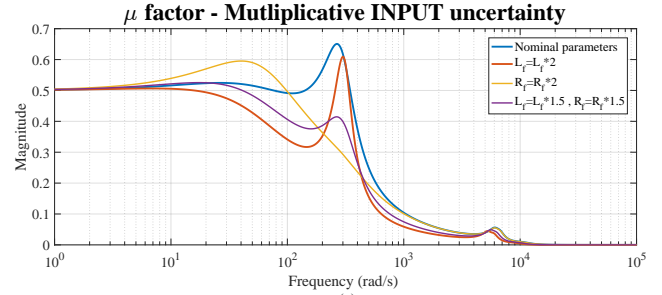


Figure 9. μ factor; (a) whole frequency range, (b) zoom. (blue) Nominal filter parameters, (red) increase of filter inductance L_f of 100%, (yellow) increase of filter resistance R_f of 100%, (violet) increase of L_f and R_f of 50%.

show clearly that the maximum peak of the μ -factor is reduced to a value of $\mu \approx 0.53$, corresponding to an increase of the stability margin. Fig. 8 shows the variation of the μ -factor for a sweep of the grid SCR from 20 to 2 when the two converters are connected in parallel and whose filter parameters, namely L_{f1} , L_{f2} , R_{f1} , and R_{f2} , have been increased of 20%. Effects of increased filter impedance on the dynamic performance of the control are shown in the section dedicated to the experimental results.

Due to the fact that converter filters are typically designed so as to optimize the trade-off between power quality and size of the filter components, a simple and efficient way for increasing the output impedance of the converter without necessarily oversizing the hardware components is represented by the emulation of a virtual impedance through the control. This represents a well-established technique in micro-grid applications and several possible solutions can be found in the literature [31]-[35]. Different techniques have been proposed for a variety of purposes, e.g. proper sharing of active and reactive power among units [32], current limitations [33] or harmonics suppression [34], [35]. Assuming that the filter impedance can be arbitrarily modified, for example by means of a virtual impedance implementation technique, in the next section, an indication about optimal parameter choice for design purposes is provided investigating the effects of converter output filter parameter variations on the μ -factor.

D. Tuning of the virtual impedance

The curves shown in Fig. 9 have been obtained varying the magnitude of the resistive and inductive components of the filter parameters shown in Table I. The blue line represents the μ -factor for the case when the two synchronverters are simply connected in parallel and their respective filters have

the nominal values shown in Table I, which coincides with the red curve of Fig. 5 and Fig. 7. Indicating with L_f the sum of L_{f1} and L_{f2} , the red curve of Fig. 9 shows the μ -factor for an increase of L_f of 100%. Although this parameter choice causes a reduction of the amplitude of the curve in almost the whole investigated frequency range, a resonance peak around the fundamental frequency can be observed. On the contrary, the same magnitude of variation applied to the filter resistance $R_f = R_{f1} + R_{f2}$ provides significant damping to the aforementioned resonance peak, whereas it produces an increase of the μ -factor in the range $\omega = [10 ; 100] \text{ rad/s}$, as indicated by the yellow line in the figure. Finally, the violet curve represents the case when the filter parameters L_{f1} , L_{f2} , R_{f1} , and R_{f2} are increased of 50%. Compared to the blue curve, this parameter choice ensures a reduction of the μ -factor in the whole investigated frequency range and provides satisfactory damping around the fundamental frequency. As it will be shown in the next section, the increase of filter impedance causes a detriment of the dynamic response of the system. Fig. 9 shows how the increase of the filter impedance enhances significantly the robust stability of the synchronverter for parallel operation with other converters of the same type. According to these considerations, it is recommended to choose the parameters of the virtual impedance such as the corresponding total filter resistance $R_f = [0.07 ; 0.15] pu$ and the total filter inductance $L_f = [0.15 ; 0.25] pu$, in order to obtain a good compromise between robustness and dynamic performances.

IV. EXPERIMENTAL RESULTS

Experimental tests in a laboratory environment have been carried out so as to validate the results of the robust stability analysis performed in this paper. The laboratory set-up used for the tests is shown in Fig. 10 (a) and (b), where a schematic drawing and a picture of the laboratory environment are shown, respectively. Two converters Danfoss Series FC-302, 4 kW rated power, operating with a switching frequency of 10 kHz and equipped with output filters have been used. Each converter is additionally equipped with a transformer in order to provide galvanic isolation. The two converters are connected to a 4-quadrant linear power amplifier PAS 15000 from Spitzenberger-Spies (single phase rated power 15 kVA, total three phase rated power 45 kVA). The control algorithms of the two converters are implemented in a dSPACE control Desk DS1202 MicroLabBox, whereas a grid model is simulated in real-time by means of an RTDS simulator. The set-up enables reproducing the simulated voltages at the output terminals of the power amplifier instantaneously for easy testing of the converters under different grid conditions.

The developed linearized model of the two synchronverters connected in parallel is validated against electromagnetic transient (EMT) time-domain simulations in MATLAB/Simulink/PLECS (modelling the converter as a voltage source) and against measurements performed with the described test set-up. Set-up parameters along with control parameters of the two synchronverters are reported in Table II. Results are shown in Fig. 11, where steps of 0.25 pu of

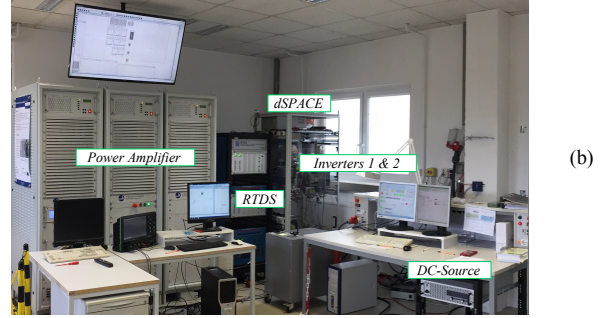
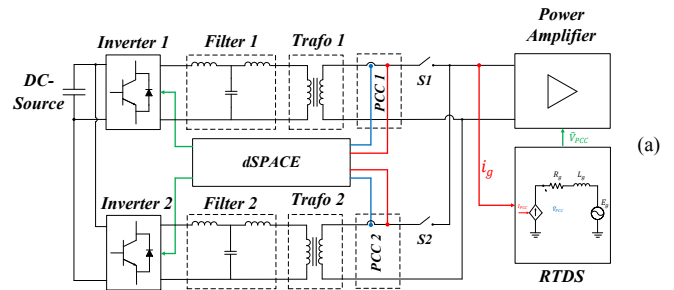


Figure 10. Experimental set-up, (a) scheme, (b) picture.

Table II
PARAMETERS EXPERIMENTAL SETUP

Description	Symbol	Value
Inverter rated power	$S_{n1}=S_{n2}$	4 kVA
Line-to-line voltage	V_{LL}	380 V (rms)
Rated grid frequency	f_g	50 Hz
Inverter switching frequency	f_{sw}	10 KHz
Grid inductance	L_g	3mH
Inverter-side filter inductance	$L_{f1I}=L_{f1II}$	5.2 mH
Grid-side filter inductance	$L_{f2I}=L_{f2II}$	0.5 mH
Transformer inductance	$L_{T1} = L_{T2}$	1.5mH
Grid resistance	R_g	1 Ω
Inverter-side filter resistance	$R_{f1I}=R_{f1II}$	2 Ω
Grid-side filter resistance	$R_{f2I}=R_{f2II}$	1 Ω
Capacitor damping resistance	$R_{cI}=R_{cII}$	5 Ω
Filter capacitor	$C_{f1}=C_{fII}$	1.5 μF
Virtual inertia	$J_1=J_2$	4e-4
Q-loop inverse integrator gain	$K_1=K_2$	800
P-Droop coefficient	$D_{p1}=D_{p2}$	0.8
Q-Droop coefficient	$D_{q1}=D_{q2}$	245

active and reactive power setpoints of the synchronverter 1 indicated as P_{set1} and Q_{set1} , respectively, are performed and the dynamic behaviour of active and reactive power output of the two converters P_1, P_2, Q_1 and Q_2 are observed. The results show a good match between simulations and measurements for quantities within the same converter, namely: $\frac{\Delta P_1}{\Delta P_{set1}}, \frac{\Delta Q_1}{\Delta Q_{set1}}$ as well as for the cross-coupling effects between active and reactive power: $\frac{\Delta Q_1}{\Delta P_{set1}}, \frac{\Delta P_1}{\Delta Q_{set1}}$. A satisfactory match between measurements and simulations can be also observed for the cross-coupling effects between the two converters: $\frac{\Delta P_1}{\Delta P_{set2}}, \frac{\Delta Q_1}{\Delta P_{set2}}, \frac{\Delta Q_1}{\Delta Q_{set2}}$.

A. Virtual impedance implementation

In order to prove the results of the analysis performed in this paper, experimental tests are reported in the following,

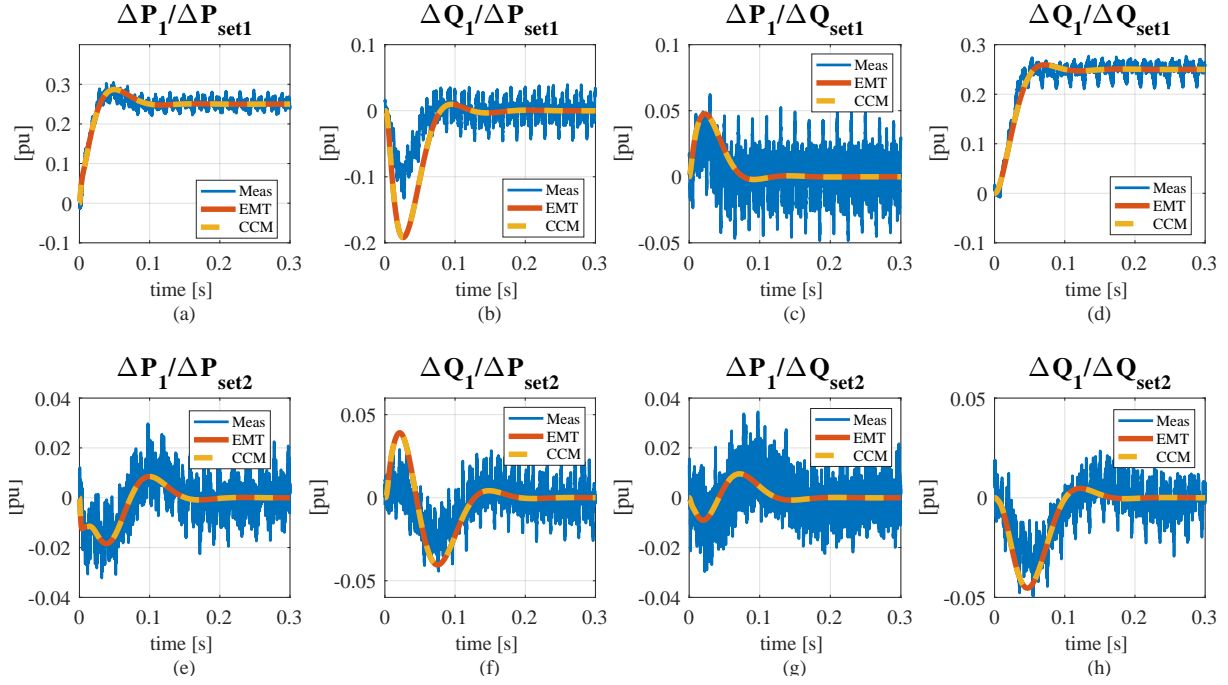


Figure 11. Comparison experimental results (blue), EMT simulations (red), linearized model (yellow). (a) $\frac{\Delta P_1}{\Delta P_{set1}}$, (b) $\frac{\Delta Q_1}{\Delta P_{set1}}$, (c) $\frac{\Delta P_1}{\Delta Q_{set1}}$, (d) $\frac{\Delta Q_1}{\Delta Q_{set1}}$, (e) $\frac{\Delta P_1}{\Delta P_{set2}}$, (f) $\frac{\Delta Q_1}{\Delta P_{set2}}$, (g) $\frac{\Delta P_1}{\Delta Q_{set2}}$, (h) $\frac{\Delta Q_1}{\Delta Q_{set2}}$.

showing the effects of the virtual impedance implementation on the robust stability of the converter. The virtual impedance implementation proposed in [6] is adopted in this work, whose principle is briefly explained below. It represents an intuitive and efficient solution for virtually increasing the filter impedance of the converter by a factor n . According to Fig. 12 (a), which shows the equivalent single phase electrical circuit of the VSM, one could imagine splitting the total impedance into a physical part, represented by the filter impedance, and a virtual additional component to be implemented in the control, whose amplitude is $(n - 1)$ times the magnitude of the filter impedance. Calculating the quantity e'_a from the equivalent scheme shown in Fig. 12(a):

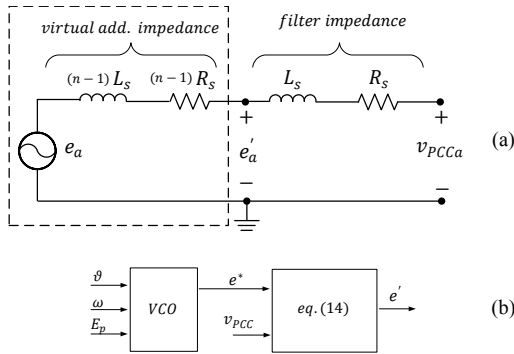


Figure 12. (a) Equivalent electrical scheme, (b) reference voltage generation block diagram.

$$e'_a = \frac{(n-1)v_{PCCa} + e_a}{n}, \quad (14)$$

where e_a represents the phase a component of the synchron-

verter virtual back-emf voltage, calculated as below [2]:

$$e^* = \begin{bmatrix} e_a \\ e_b \\ e_c \end{bmatrix} = E_p \omega \begin{bmatrix} \sin(\theta) \\ \sin(\theta - \frac{2}{3}\pi) \\ \sin(\theta - \frac{4}{3}\pi) \end{bmatrix}. \quad (15)$$

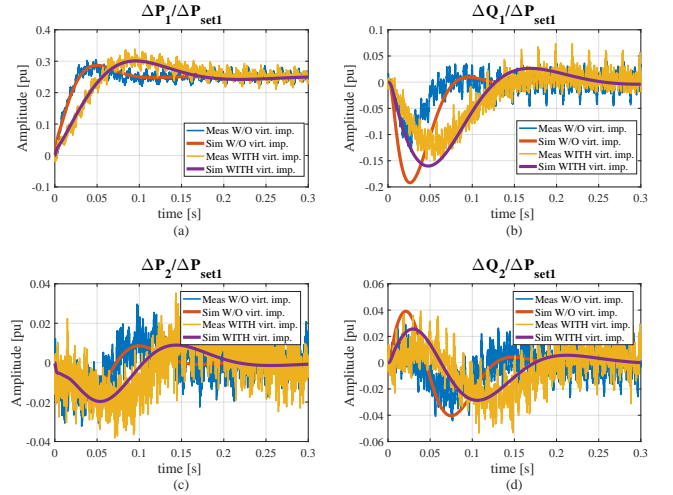


Figure 13. Comparison experimental results vs. EMT simulations. (blue) measurements without virtual impedance implementation, (red) simulations without virtual impedance implementation, (yellow) measurements with virtual impedance implementation, (violet) simulations with virtual impedance implementation. (a) $\frac{\Delta P_1}{\Delta P_{set1}}$, (b) $\frac{\Delta Q_1}{\Delta P_{set1}}$, (c) $\frac{\Delta P_2}{\Delta P_{set1}}$, (d) $\frac{\Delta Q_2}{\Delta P_{set1}}$.

The effects of the additional impedance are reproduced by imposing the calculated e'_a for the generation of the converter pulses in Fig.1. In Fig. 13, measurements results are compared to EMT simulations. According to the considerations about the optimal filter tuning presented in section III.D, the approach

- [4] P. Rodriguez, C. Citro, I. Candela, J. Rocabert, and P. Rodriguez, "Flexible grid connection and islanding of SPC-based PV power converters," *IEEE Trans. Ind. Appl.*, 2018, DOI 10.1109/TIA.2018.2800683.
- [5] L. Zhang, L. Harnefors, and H. P. Nee, "Power Synchronization Control of Grid-Connected Voltage Source Converters," *IEEE Trans. Power Systems*, vol. 25, no. 2, pp. 809-820, May 2010.
- [6] V. Natarajan and G. Weiss, "Synchronverters with better stability due to virtual inductors, virtual capacitors and anti wind-up," *IEEE Trans. Ind. Electron.*, vol. 64, no. 7, pp. 5994-6004, Jul. 2017.
- [7] B. Wen, D. Boroyevich, R. Burgos, P. Mattavelli, and Z. Shen, "Analysis of D-Q Small-Signal Impedance of Grid-Tied Inverters," *IEEE Trans. Power Electron.*, vol. 31, no. 1, pp. 675-687, Mar. 2016.
- [8] L. Harnefors, M. Bongiorno, and S. Lundberg, "Input-Admittance Calculation and Shaping for Controlled Voltage-Source Converters," *IEEE Trans. Ind. Electron.*, vol. 54, no. 6, pp. 3323-3334, Dec. 2007.
- [9] R. Rosso, G. Buticchi, M. Liserre, Z. Zou and S. Engelken, "Stability analysis of synchronization of parallel power converters," in *Proc. 43rd Annual Conference of the IEEE Industrial Electronics Society IECON 2017*, Beijing, China, 2017, pp. 440-445.
- [10] R. Rosso, J. Cassoli, S. Engelken, G. Buticchi, and M. Liserre, "Analysis and design of LCL filter based synchronverter", in *Proc. 2017 IEEE Energy Conversion Congress and Exposition (ECCE)*, Cincinnati, OH, 2017, pp. 5587-5594.
- [11] H. Wu, X. Ruan, D. Yang, X. Chen, W. Zhao, Z. Lv, and Q.-C. Zhong, "Small-signal modeling and parameters design for virtual synchronous generators," *IEEE Trans. Ind. Electron.*, vol. 63, no. 7, pp.4292-4303, Jul. 2016.
- [12] S. Dong and Y. C. Chen, "A method to directly compute synchronverter parameters for desired dynamic response," *IEEE Trans. Power Electron.*, 2017, DOI: 10.1109/TEC.2017.2771401
- [13] R. Aouini, B. Marinescu, K. B. Kilani, and M. Elleuch, "Synchronverter-based emulation and control of HVDC transmission," *IEEE Trans. Power Syst.*, vol. 31, no. 1, pp. 278286, Jan. 2016.
- [14] S. Dong and Y. C. Chen, "Adjusting Synchronverter dynamic response speed via damping correction loop", *IEEE Trans. Energy Conv.*, Vol. 32, no. 2, pp.608-619, July 2017.
- [15] X. Wang, F. Blaabjerg, and W. Wu, "Modeling and analysis of harmonic stability in an AC power-electronics-based power system," *IEEE Trans. Ind. Electr.*, Vol. 29, no. 12, pp.6421-6432, December 2014.
- [16] J. Sun, "Small-Signal Methods for AC Distributed Power Systems-A Review," *IEEE Trans. Power Electron.*, Vol. 24, no. 11, pp.2545-2553, November 2009.
- [17] M. Amin and M. Molinas, "Self-synchronization of wind farms in MMC-based HVDC system," in *Proc. 2016 IEEE Electrical Power and Energy Conference (EPEC)*, Ottawa, ON, 2016, pp. 1-6.
- [18] S. Skogestad and I. Postlethwaite, "Multivariable feedback control - analysis and design", Wiley and Sons, 2001.
- [19] K. Zhou and J. C. Doyle, "Essentials of robust control", Upper Saddle River: NJ. Prentice-Hall, 1998.
- [20] R. Rosso, J. Cassoli, G. Buticchi, S. Engelken, and M. Liserre, "Robust stability analysis of LCL filter based synchronverter under different grid conditions," *IEEE Trans. Power Electron.*, 2018, DOI 10.1109/TPEL.2018.2867040.
- [21] L. Jessen, Z. Zou, B. Benkendörff, M. Liserre, and F. W. Fuchs, "Resonance identification and damping in AC-grids by means of multi MW grid converters," in *Proc. 42nd Annual Conference of the IEEE Industrial Electronics Society (IECON)*, Florence, 2016, pp. 3762-3768.
- [22] Z. Shuai, Y. Hu, Y. Peng, C. Tu, and Z. J. Shen, "Dynamic-stability analysis of synchronverter-dominated microgrid based on bifurcation theory," *IEEE Trans. on Ind. Electr.*, vol. 64, no.9, pp. 7467-7477, Sept.2017.
- [23] R. Rosso, S. Engelken, and M. Liserre, "Analysis of the behavior of synchronverters operating in parallel by means of component connection method," in *Proc. 2018 IEEE Energy Conversion Congress and Exposition (ECCE)*, Portland, OR, 2018.
- [24] G. Gaba, S. Lefebvre, and D. Mukhedkar, "Comparative analysis and study of the dynamic stability of AC/DC systems," *IEEE Trans. Power Systems*, vol. 3, no. 3, pp. 978-985, Aug. 1988.
- [25] P. Kundur, "Power System Stability and Control", McGraw-Hill, Inc. 1994.
- [26] X. Wang, F. Blaabjerg, M. Liserre, Z. Chen, J. He, and Y. Li, "An Active Damper for Stabilizing Power-Electronics-Based AC Systems," *IEEE Trans. Power Electron.*, vol. 29, no. 7, pp. 3318-3329, Jul. 2014.
- [27] X. Wang and F. Blaabjerg, "Harmonic Stability in Power Electronic Based Power Systems: Concept, Modeling, and Analysis," *IEEE Trans. Smart Grids*, DOI: 10.1109/TSG.2018.2812712.
- [28] J. Rocabert, A. Luna, F. Blaabjerg, and P. Rodriguez, "Control of power converters in AC microgrids," *IEEE Trans. Power Electron.*, vol. 27, no. 11, Nov. 2012, pag. 4734, 4749.
- [29] E. Ebrahimzadeh, F. Blaabjerg, X. Wang, C. L. Bak, "Harmonic instability source identification in large wind farms," in *Proc. 2017 IEEE Power & Energy Society General Meeting*, Chicago, IL, 2017.
- [30] R. Rosso, S. Engelken, and M. Liserre, "A generalized formulation of active power synchronization based control algorithms for grid connected converters," in *Proc. 44th Annual Conference of the IEEE Industrial Electronics Society IECON 2018*, Washington DC., 2018.
- [31] X. Wang, Y. W. Li, F. Blaabjerg, and P. C. Loh, "Virtual-impedance-based control for voltage-source and current-source converters," *IEEE Trans. Power Electron.*, vol. 30, no. 12, pp. 7019-7037, Dec. 2015.
- [32] M. Hua, H. Hu, Y. Xing, and J. Guerrero, "Multilayer control for inverters in parallel operation without intercommunications," *IEEE Trans. Power Electron.*, vol. 27, no. 8, pp. 3651-3663, Aug. 2012.
- [33] X. Lu, J. Wang, J.M. Guerrero, and D. Zhao, "Virtual impedance based fault current limiters for inverter dominated AC microgrids," *IEEE Trans. Smart Grid*, 2016, DOI 10.1109/TSG.2016.2594811.
- [34] A. Terraso, J. I. Candela, J. Rocabert, and P. Rodriguez, "Grid voltage harmonic damping method for SPC based power converters with multiple virtual admittance control," in *Proc. IEEE Energy Conv. Congr. and Exp. (ECCE)*, Cincinnati, OH, 2017, pp. 64-68.
- [35] X. Lu, J. Wang, J. M. Guerrero, and D. Zhao, "An islanding micro-grid power sharing approach using enhanced virtual impedance control," *IEEE Trans. Power Electron.*, vol. 28, no. 11, pp. 5272-5282, Nov. 2013.



Roberto Rosso (S'17) received the B.Sc. degree in electronic engineering and the M.Sc. degree in electrical engineering in 2009 and 2012, respectively, from the University of Catania, Catania, Italy. He is currently working toward the Ph.D. degree (since 2017) in electrical engineering at the Christian-Albrechts-University of Kiel, Kiel, Germany. In 2013, he joined the R & D division of the wind turbine manufacture ENERCON (Wobben Research and Development WRD), where he is currently working at the Control Engineering Department. He has been involved in several research projects addressing analytical models of electrical machines and control of electric drive systems. His research interests include control strategies for grid integration of renewable energy systems.



Soenke Engelken (S'08-M'12) is the Head of Control Engineering at WRD Wobben Research and Development. The Control Engineering department develops control solutions for wind energy converters, spanning wind turbine controls, electrical systems controls and grid-side converter controls. Prior to joining Wobben Research and Development, he received his Ph.D. and M.Sc. degrees in control engineering from the University of Manchester, UK, in 2012 and 2008, respectively, as well as his B.Sc. degree in electrical engineering and computer science from Jacobs University Bremen, Germany, in 2007. He is a member of the IEEE Power and Energy Society, the IEEE Control Systems Society, of CIGR Joint Working Group A1/C4.52 Wind Generators and Frequency-Active Power Control and of the ENTSO-E Expert Group on High Penetration Issues.



Marco Liserre (S'00-M'02-SM'07-F'13) received the MSc and PhD degree in Electrical Engineering from the Bari Polytechnic, respectively in 1998 and 2002. He has been Associate Professor at Bari Polytechnic and Professor at Aalborg University (Denmark). He is currently Full Professor and he holds the Chair of Power Electronics at Christian-Albrechts-University of Kiel (Germany). He has published over 300 technical papers (more than 86 of them in international peer-reviewed journals) and a book. These works have received more than 20000 citations. Marco Liserre is listed in ISI Thomson report The worlds most influential scientific minds.